ASTRONOMY & ASTROPHYSICS
SUPPLEMENT SERIES

FEBRUARY II **2000**, PAGE 85

Astron. Astrophys. Suppl. Ser. **142**, 85–94 (2000)

Recombination coefficients for C II lines⋆

A.R. Davey[1], **P.J. Storey**[2], **and R. Kisielius**[2]

[1] Department of Physics, Montana State University, Bozeman, MT 59717-3840, U.S.A.
e-mail: ard@filament.physics.montana.edu
[2] Department of Physics and Astronomy, University College London, Gower St., London, WC1E 6BT, UK
e-mail: rk@star.ucl.ac.uk, pjs@star.ucl.ac.uk

Received July 20; accepted October 4, 1999

Abstract. Effective recombination coefficients are given for C II transitions between doublet states. The calculations are carried out in the temperature range $500 - 20\,000$ K and for an electron density of 10^4 cm^{-3}. The effects of electron collisions on the excited states are included. The necessary bound-bound and bound-free radiative data are obtained from a new R-matrix calculation in which photoionization resonances are fully delineated, thereby accurately incorporating the effects of both radiative and dielectronic recombination. The R-matrix calculation includes all bound states with principal quantum number $n \leq 15$ and total orbital angular momentum $L \leq 4$. The effect of moving the resonance features to their experimentally determined positions is also investigated and found to be important at low temperatures.

Key words: atomic data — line: formation — H II regions — planetary nebulae: general

1. Introduction

This is the third in a series of papers dealing with the theoretical recombination spectra of once ionized abundant elements, with the previous two papers dealing with O II (Storey 1994) and Ne II (Kisielius et al. 1998). In this paper, as in the earlier papers, we calculate theoretical recombination line intensities making use of high quality bound-bound and bound-free radiative data calculated using the techniques developed for the Opacity Project (OP) (Seaton 1987; Berrington et al. 1987). This entails the use of the R-matrix method to solve the Schrödinger equation in the close-coupling approximation of electron-ion collision theory. The radiative data deposited in the OP database (Cunto et al. 1993) for photoionization of C^+, however, is tabulated at too coarse a mesh for recombination work, so an improved calculation of these data is described in this paper (Sect. 2). In this approach, autoionizing states appear as resonances in the photoionization cross-sections and effects such as the mean free electron energy being comparable to the resonance widths and non-zero background cross-sections between resonances are correctly treated. The omission of these effects can significantly affect the recombination coefficients at low temperature (Nussbaumer & Storey 1983). We also discuss the problem of radiative damping of resonances (Kisielius et al. 1998).

The case of C II differs from the ions previously discussed in that there is extensive, although not complete, experimental information (Moore 1970) about the positions of autoionizing states lying close to the C^+ ionization threshold, which are responsible for the process of low-temperature dielectronic recombination (Storey 1981, 1982). These experimental data enable us to empirically correct the calculated positions of these states, which appear as resonances in the calculated photoionization cross-sections (Sect. 2.4).

The calculation described here deals only with the doublet states of C^+. There are also quartet states converging on the 2s2p (^{3}P^o) state of C^{2+}, but these can only be populated by direct recombination from the C^{2+} 2s2p (^{3}P^o) state or by dielectronic recombination through quartet autoionizing states. At nebular temperatures ($T \leq 20\,000$ K), there will not be significant population in the C^{2+} 2s2p (^{3}P^o) state so direct recombination to the quartets will be insignificant. The quartet autoionizing states can only autoionize through weak spin-orbit (and other weak relativistic) interactions with doublet autoionizing states, since there is no quartet continuum available. Such interactions are weak among the states just above the ionization threshold, so we do not expect the quartet states to

Send offprint requests to: P.J. Storey

⋆ Tables 1–5 are also available in electronic form at the CDS via anonymous ftp to cdsarc.u-strasbg.fr (130.79.128.5) or via http://cdsweb.u-strasbg.fr/Abstract.html

have any significant effect on the intensities of the doublet lines treated here. Recombination lines from quartet states are nonetheless observed, even at nebular temperatures. For a treatment of dielectronic recombination through the doublet and quartet states see Badnell (1988).

The term structure of C^+ also differs from that of O^+ and Ne^+ in that due to the zero spin and orbital angular momentum of the C^{2+} ^1S state, each valence orbital only gives rise to one atomic term usually with negligible fine-structure. As a result, there are fewer recombination lines and they are of much greater intensity than in O II and Ne II. It is therefore possible to detect recombination lines of C II from higher principal quantum numbers than for the other two ions, and this opens up the possibility of testing the theory for a greater range of ionic states (Liu et al. 2000). Our tabulated results are consequently also more extensive. We also extend the calculations to lower temperatures ($\geq$ 500 K) following the observation of the 1335 Å and 4267 Å lines from an old nova remnant (Ferland et al. 1984).

Recombination lines of C II are also seen in the spectra of the stellar winds of Wolf-Rayet central stars of planetary nebulae (DeMarco et al. 1998) where particle densities are much higher than in PN. In a further paper, we will present a theoretical treatment of the C II recombination spectrum at high density, where collisional processes become important.

2. The R-matrix calculation

2.1. C^{2+} target

We calculate the the bound-bound and bound-free radiative data for C^+ states from a $C^{2+} + e^-$ scattering problem. The starting point for the calculations is the C^{2+} target. In our photoionization calculations, as in the OP calculations (Yu Yan & Seaton 1987), the C^{2+} target given by Berrington et al. (1977) was used. It includes the $2s^2\ ^1S^e$, $2s2p\ ^3P^o$, $^1P^o$ and $2p^2\ ^3P^e$, $^1D^e$, $^1S^e$ target eigenstates represented in terms of seven orthogonal basis orbitals and pseudo-orbitals: 1s, 2s, 2p, $\bar{3}$s, $\bar{3}$p, $\bar{3}$d, $\bar{4}$f. The radial parts of the basis orbitals were obtained using the CIV3 code of Hibbert (1975).

2.2. C^+ bound state energies

We have calculated ionization energies for all doublet states with total orbital angular momentum quantum number $L \leq 4$ and with principal quantum number $n \leq 15$. These energies are compared with existing experimental energies in Tables 1 and 2. Note that the main $2s^2nl$ series states are perturbed by states from the 2s2p3s and 2s2p3p electron configurations. The upper principal quantum number limit ($n \leq 15$) of the present calculation

Table 1. Energies of even parity C^+ bound states relative to the ionization threshold

State	Energy (Ry) Calculated	Experimental
	$^2S^e$	
$2s2p^2$	−0.899095	−0.912867
$2s^23s$	−0.725740	−0.730205
$2s^24s$	−0.358483	−0.359335
$2s^25s$	−0.212136	−0.212489
$2s^26s$	−0.140152	−0.140346
$2s^27s$	−0.099483	−0.099622
$2s^28s$	−0.074279	
$2s^29s$	−0.057592	
$2s^210s$	−0.045989	
$2s^211s$	−0.037622	
$2s^212s$	−0.031477	
2s2p3p	−0.027270	
$2s^213s$	−0.024921	
$2s^214s$	−0.022077	
$2s^215s$	−0.019253	
	$^2P^e$	
$2s2p^2$	−0.767228	−0.783844
2s2p3p	−0.131191	−0.133305
	$^2D^e$	
$2s2p^2$	−1.10066	−1.10937
$2s^23d$	−0.463932	−0.465812
$2s^24d$	−0.259290	−0.260092
$2s^25d$	−0.165203	−0.165578
$2s^26d$	−0.114471	−0.114731
$2s^27d$	−0.084449	
2s2p3p	−0.070199	−0.073480
$2s^28d$	−0.062318	
$2s^29d$	−0.049872	
$2s^210d$	−0.040445	
$2s^211d$	−0.033420	
$2s^212d$	−0.028068	
$2s^213d$	−0.023903	
$2s^214d$	−0.020599	
$2s^215d$	−0.017934	
	$^2G^e$	
$2s^25g$	−0.160169	−0.160314
$2s^26g$	−0.111251	−0.111320
$2s^27g$	−0.081734	−0.081775
$2s^28g$	−0.062574	−0.062612
$2s^29g$	−0.049437	
$2s^210g$	−0.040041	
$2s^211g$	−0.033089	
$2s^212g$	−0.027802	
$2s^213g$	−0.023688	
$2s^214g$	−0.020424	
$2s^215g$	−0.017791	

Table 2. Energies of odd parity C^+ bound states relative to the ionization threshold

State	Energy (Ry) Calculated	Experimental
	$^2P^o$	
$2s2p^2$	−1.78778	−1.79184
$2s^23p$	−0.589943	−0.591739
$2s^24p$	−0.310095	−0.311142
$2p^3$	−0.245582	−0.254462
$2s^25p$	−0.190823	−0.194769
2s2p3s	−0.166010	−0.172032
$2s^26p$	−0.124169	−0.124589
$2s^27p$	−0.090202	−0.090391
$2s^28p$	−0.068281	
$2s^29p$	−0.053445	
$2s^210p$	−0.042958	
$2s^211p$	−0.035277	
$2s^212p$	−0.029484	
$2s^213p$	−0.025008	
$2s^214p$	−0.021479	
$2s^215p$	−0.018647	
	$^2D^o$	
$2p^3$	−0.413724	−0.421035
	$^2F^o$	
$2s^24f$	−0.252011	−0.252308
$2s^25f$	−0.161223	−0.161382
$2s^26f$	−0.111882	−0.112070
$2s^27f$	−0.082144	−0.082228
$2s^28f$	−0.062855	
$2s^29f$	−0.049638	
$2s^210f$	−0.040189	
$2s^211f$	−0.033202	
$2s^212f$	−0.027890	
$2s^213f$	−0.023758	
$2s^214f$	−0.020480	
$2s^215f$	−0.017836	

was chosen to include the 2s2p3p ^2S term which lies energetically between the 12s $^2S^e$ and 13s $^2S^e$ terms. This perturbation is not included in the OP calculation for C^+, which only extends to $n = 10$. Such perturbations significantly modify the photoionization cross-sections and hence recombination coefficients for nearby states in the main series.

2.3. C^+ bound-bound radiative transitions

We have described most of the techniques that we use to calculate bound-bound radiative data elsewhere (Kisielius et al. 1998). Briefly, for $n \leq 15$, $L \leq 4$, all radiative transition probabilities are obtained from the R-matrix calculation referred to above. For most other transitions we use a combination of the Coulomb approximation and hydrogenic data, the methods and codes used having been described by Storey (1994). For transitions $n \leftrightarrow n', n < n'$ with $n \leq 5$ and $n' \geq 16$ we use the following further technique. Using the R-matrix approach, photoionization cross-section data from a given lower term (S_iL_i) to a specific final symmetry (S_fL_f) can be computed for negative free electron energies, enabling us to obtain absorption oscillator strengths from the given lower term to high members of the $2s^2nl(S_fL_f)$ series. This technique has the advantage over other approximate methods, such as the Coulomb approximation, that configuration interaction is fully accounted for in the wave function of the lower term. Cascading from high Rydberg states to the low-lying terms of the ion is therefore more accurately treated.

2.4. C^+ photoionization cross-sections

In many cases treated by the OP, the free electron energy mesh on which the photoionization cross-sections are calculated, was too coarse to accurately map narrow resonance features. This usually leads to significant contributions to the recombination coefficient being missing, since the resonance contribution is proportional to the area underneath the resonance. The photoionization cross-sections for C^+ generated for the OP (Yu Yan & Seaton 1987) have poor resolution in some of the resonance structure because they were based on a mesh in which points are equally spaced in effective quantum number relative to the next threshold (hereafter referred to as a quantum defect mesh). One hundred points were provided per integer change in effective quantum number and subsequently, this number was further reduced by removing any points that could be linearly interpolated from two adjacent points within some prescribed accuracy.

In contrast to the OP data, we use a variable step energy mesh for photoionization cross-sections that delineates all resonances to a prescribed accuracy. First, we employ quantum defect theory to determine resonance positions and widths using a coarse energy mesh. We then use this information to generate an electron energy mesh which maps the resonances to a chosen accuracy (Kisielius et al. 1998). In the third step we calculate photoionization cross-sections using the new variable step mesh.

In Fig. 1, we demonstrate the difference in resolution between an OP cross-section and one calculated by our method. The OP cross section consists of 199 points based on a quantum defect mesh whilst the latter is based on an energy mesh of 3281 points. In the OP cross-section, the resonance at 1.135 Ry consists only of 3 points, and the next one is missing completely. There is a significant difference in the peak heights of the resonances too.

The effects of correctly delineating the resonances are more clearly demonstrated in Fig. 2. We show the area under the cross-sections which is a more important measure of their contribution to the recombination coefficient. The total area under the $2s2p^2$ $^2D^e$ photoionization

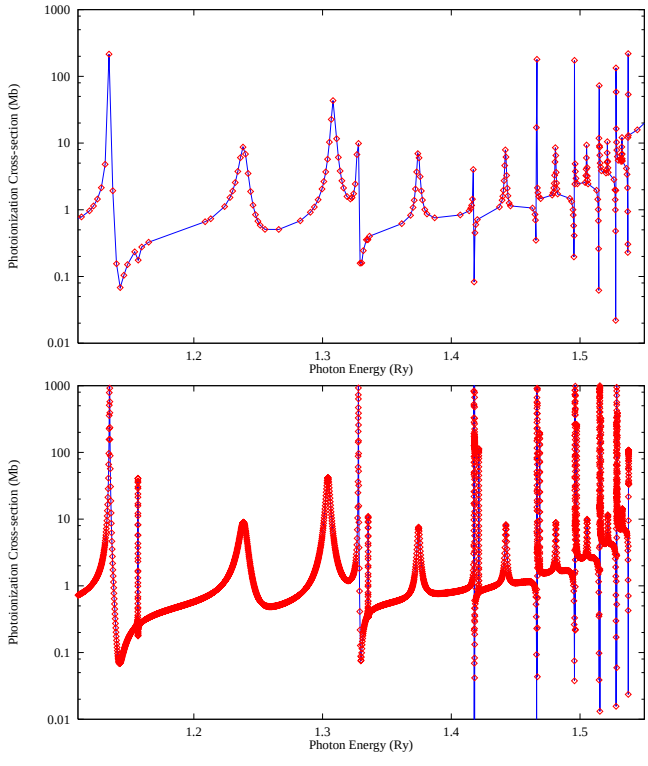

Fig. 1. Comparison of the photoionization cross-section (in Mb) for $2s2p^2\ ^2D$, calculated by the OP (top) and this work (bottom)

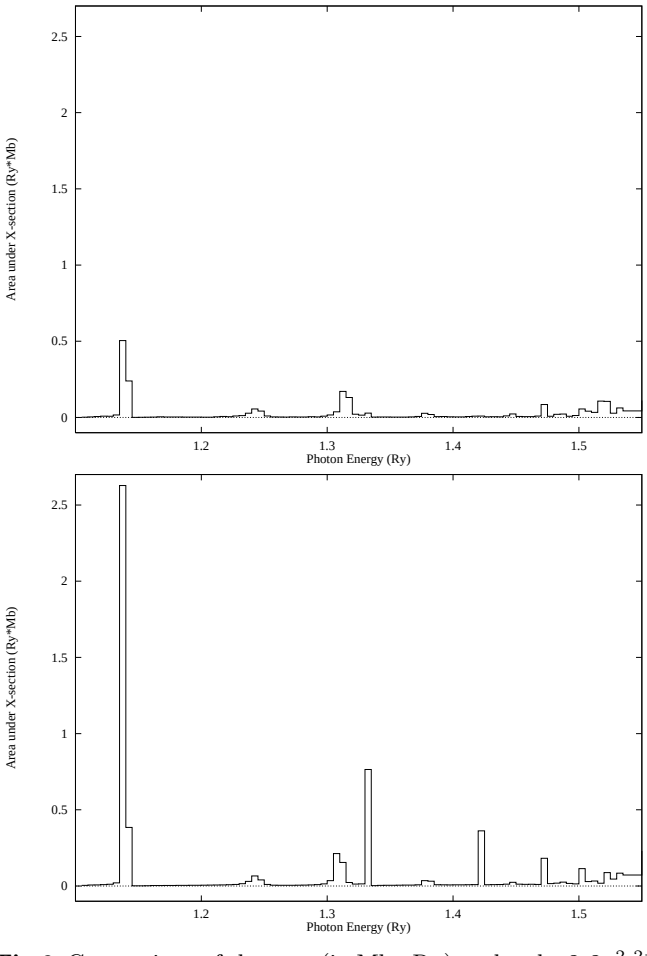

Fig. 2. Comparison of the area (in Mb · Ry) under the $2s2p^2\ ^2D$ cross-section. Top figure - OP data, bottom - present calculation

cross-section from the OP is 1.585 Mb Ry, whereas our calculation gives 4.573 Mb Ry for the same energy range.

This detailed treatment of the energy mesh was undertaken for the energy region from the $2s^2(^1S^e)$ limit up to $4/15^2$ Ry below the $2s2p(^3P^o)$ threshold, since this region contains the main contribution to the recombination at the temperatures of interest. Above the $2s2p(^3P^o)$ threshold, a quantum defect mesh was used. A very high degree of accuracy is not required here so a step in effective quantum number was chosen that provided 1000 points per integer change in quantum number.

Finally, we note that we deal with radiative damping of resonances in the same way as described by Kisielius et al. (1998), in that any autoionizing states for which the radiative width is greater than the autoionization width are omitted from the list of resonances used to generate the high resolution energy mesh. As a result such resonances do not appear in the photoionization cross-sections and do not contribute to the recombination. In practice this means omitting all resonances associated with $2s2p(^3P^o)nh$ electron configurations, as well as the $^2H^o$ terms from the $2s2p(^3P^o)ng$ configurations.

3. Recombination coefficients

An accurate treatment of the radiative-cascade problem requires detailed calculations of recombination into excited states. Few detailed photoionization calculations had been performed for $n > 2$ states, before the work of the OP. It has been noted (Storey 1982) that, in C^+, the dominant contribution to the recombination coefficient of the $2s2p^2\ ^2D^e$ state comes from the $2s2p(^3P^o)3d\ ^2F^o$ resonance. It is not only an important source of recombination for this state, but for the whole ion, particularly at low temperatures when the average free electron energy lies close to threshold. The $2s2p(^3P^o)3d\ ^2P^o$ resonance, although higher in energy is also a significant source of recombination.

In general, the theoretically calculated energies of states are higher than the experimental values. For low temperature recombination work, the placement of resonances is critical. A change in the position of the resonances can lead to a large change in the the value of the total recombination coefficient if the average free electron energy is lower than the resonance energy.

The experimentally determined positions of the $^2F^o$ and $^2P^o$ resonances (Moore 1970) are 3301 cm^{-1} and 5523 cm^{-1} above the $2s^2$ ($^1S^e$) threshold. This compares with the theoretically calculated values of 3778 cm^{-1}

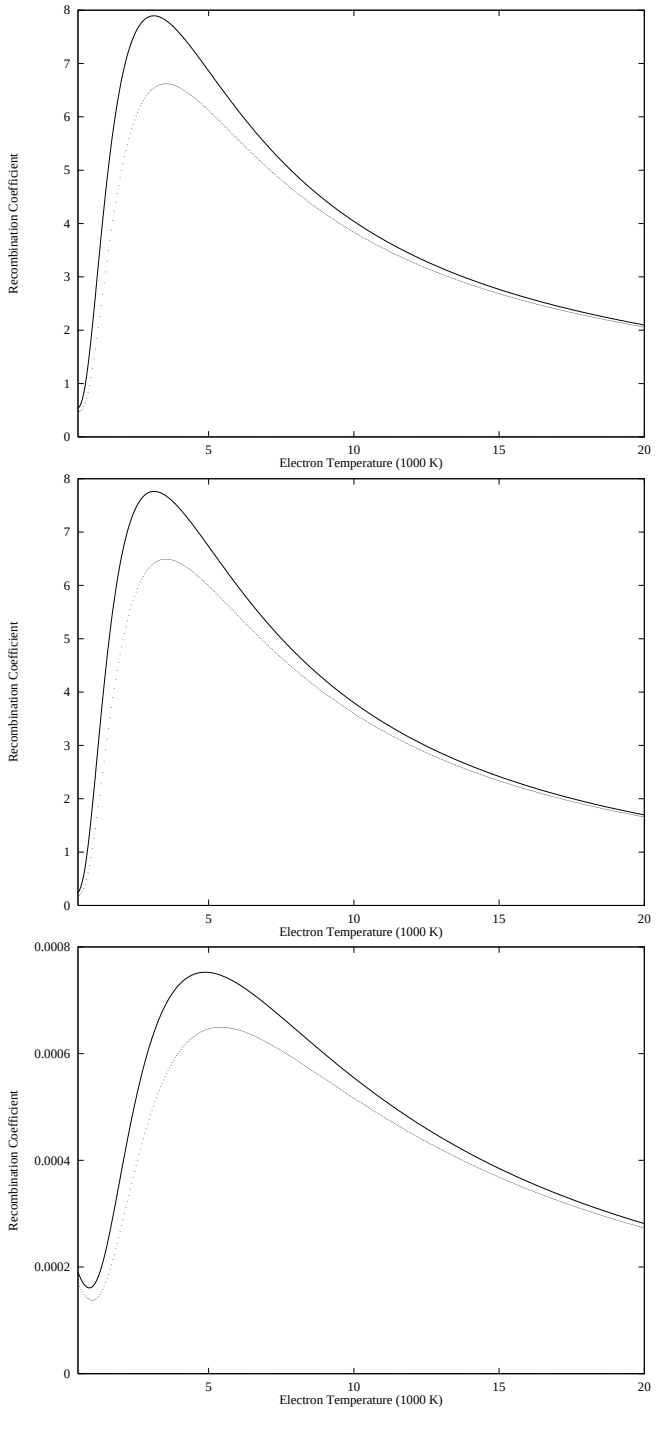

Fig. 3. The effect of moving the ^{2}F^o and ^{2}P^o resonances on the recombination coefficient (in 10^{-12} cm^3 s^{-1}) of the 2s2p^2 ^{2}D^e state. The solid lines represent recombination coefficients calculated with experimental energies for the resonances, the dotted lines – with calculated energies. The top figure shows the effect on the total recombination coefficient of moving both resonances; the centre figure shows the contribution only from the ^{2}F^o resonance; the lower figure shows the contribution only from the ^{2}P^o resonance

and 6172 cm^{-1}. We evaluate the resonance contributions to the total recombination coefficient using their experimental rather than the theoretical energies by, in effect, moving these two resonances.

This is done by fitting the photoionization cross-section in the energy region around the resonances using a Fano profile (Fano 1961). For a resonance superimposed on a constant background the profile is given by

$$F(x) = \beta + \alpha \frac{(x+q)^2}{(1+x^2)}. \quad (1)$$

The value of β can be estimated from the minimum point, $x = -q$, since then $F(x) = \beta$.

This form does not allow for any energy dependence in the background, and therefore can only be used to fit a narrow energy range. The theoretical position and width of the resonance are used to start an iterative procedure to determine the quantities q, β and α. A new profile is then generated, differing only in the energy of the peak of the profile, and integrated to give a new value of the contribution to the recombination coefficient from the resonance and the adjacent energy region. Using the new profile gives a modified recombination coefficient for the state with the resonance contributions evaluated at their experimental positions. This method was applied to all cross-sections in which the two resonances appeared, for all states $n \leq 10$. In Fig. 3, we compare the recombination coefficients for the 2s2p^2 ^{2}D^e term computed with the two lowest lying resonances in their calculated and experimentally determined positions. There are significant changes to the recombination coefficients as a result, particularly at low electron temperatures. For example, the placement of the 2s2p(^{3}P^o)3d ^{2}F^o, ^{2}P^o resonances at their experimental positions brings about a 63% increase in the recombination coefficient of the 2s2p^2 ^{2}D^e state at 1000 K.

The total recombination coefficient of a state depends, in general, on the relative populations of the C^{2+} 2s^2(^{1}S) and 2s2p(^{3}P^o) states. For the temperature and density range under consideration here, the fraction of the population in the 2s2p(^{3}P^o) state is always less than 0.01% and so we ignore recombination from this state in the present calculation.

4. Results and discussion

The population structure of C$^+$ has been calculated for the electron temperatures in the range from 500 K to 20 000 K and for electron densities below 10^6 cm^{-3}. Calculations for higher densities were also performed, including a full treatment of electron collisional processes between excited states, but this will be the subject of a subsequent paper. In the present work, we also use a full treatment of collisional processes but at the relatively low densities considered here, there is no significant difference between the full treatment and the more approximate

Table 3. Effective recombination coefficients [10^{-14} cm^3 s^{-1}] for temperature range $T_e = 3500 - 20\,000$ K. Electron density $N_e = 10^4$ [cm^{-3}]. Minimum recombination coefficient $\alpha_{min} = 3.0$

Transition			λ[nm]	Case	T_e [1000 K] 3.5	5.0	7.5	10.0	12.5	15.0	20.0
8h (^{2}H^o)	–	6g (^{2}G^e)	1866.2	A	3.52+0	2.44+0	1.57+0	1.13+0	8.71−1	6.99−1	4.90−1
8h (^{2}H^o)	–	5g (^{2}G^e)	931.4	A	3.19+0	2.22+0	1.43+0	1.03+0	7.90−1	6.34−1	4.44−1
7h (^{2}H^o)	–	6g (^{2}G^e)	3068.8	A	8.18+0	5.58+0	3.52+0	2.51+0	1.91+0	1.52+0	1.05+0
7h (^{2}H^o)	–	5g (^{2}G^e)	1157.9	A	7.82+0	5.33+0	3.37+0	2.39+0	1.82+0	1.45+0	1.01+0
7g (^{2}G^e)	–	5f (^{2}F^o)	1144.4	A	4.23+0	3.05+0	2.06+0	1.53+0	1.21+0	9.97−1	7.80−1
7g (^{2}G^e)	–	4f (^{2}F^o)	534.2	A	5.07+0	3.66+0	2.47+0	1.84+0	1.45+0	1.20+0	9.35−1
7f (^{2}F^o)	–	3d (^{2}D^e)	237.5	A	3.28+0	2.50+0	1.81+0	1.42+0	1.17+0	1.02+0	9.61−1
				B	3.33+0	2.55+0	1.85+0	1.45+0	1.20+0	1.04+0	9.84−1
7d (^{2}D^e)	–	3p (^{2}P^o)	179.6	A	3.82−1	3.16−1	2.49−1	2.08−1	1.81−1	1.64−1	1.55−1
				B	3.93+0	3.25+0	2.56+0	2.14+0	1.86+0	1.68+0	1.59+0
6h (^{2}H^o)	–	5g (^{2}G^e)	1851.6	A	3.03+1	2.00+1	1.22+1	8.53+0	6.40+0	5.04+0	3.44+0
6g (^{2}G^e)	–	5f (^{2}F^o)	1819.9	A	9.74+0	6.88+0	4.53+0	3.32+0	2.59+0	2.12+0	1.65+0
6g (^{2}G^e)	–	4f (^{2}F^o)	646.2	A	1.26+1	8.88+0	5.85+0	4.29+0	3.35+0	2.74+0	2.13+0
6f (^{2}F^o)	–	4d (^{2}D^e)	615.1	A	3.97+0	2.99+0	2.14+0	1.66+0	1.36+0	1.17+0	1.08+0
				B	4.03+0	3.05+0	2.18+0	1.69+0	1.39+0	1.20+0	1.11+0
6f (^{2}F^o)	–	3d (^{2}D^e)	257.5	A	6.63+0	5.01+0	3.57+0	2.78+0	2.28+0	1.96+0	1.81+0
				B	6.74+0	5.09+0	3.64+0	2.83+0	2.32+0	2.01+0	1.86+0
6d (^{2}D^e)	–	3p (^{2}P^o)	191.0	A	5.56−1	4.50−1	3.48−1	2.88−1	2.48−1	2.21−1	2.05−1
				B	6.41+0	5.18+0	4.01+0	3.32+0	2.85+0	2.55+0	2.37+0
5g (^{2}G^e)	–	4f (^{2}F^o)	990.3	A	5.07+1	3.44+1	2.17+1	1.55+1	1.18+1	9.56+0	7.31+0
5f (^{2}F^o)	–	4d (^{2}D^e)	923.0	A	9.16+0	6.76+0	4.70+0	3.58+0	2.90+0	2.47+0	2.21+0
				B	9.28+0	6.86+0	4.78+0	3.65+0	2.95+0	2.52+0	2.25+0
5f (^{2}F^o)	–	3d (^{2}D^e)	299.3	A	1.76+1	1.30+1	9.02+0	6.88+0	5.56+0	4.74+0	4.23+0
				B	1.78+1	1.32+1	9.16+0	7.00+0	5.66+0	4.83+0	4.33+0
5d (^{2}D^e)	–	3p (^{2}P^o)	213.8	A	9.07−1	7.24−1	5.54−1	4.54−1	3.88−1	3.46−1	3.18−1
				B	1.25+1	9.96+0	7.62+0	6.25+0	5.34+0	4.76+0	4.39+0
4f (^{2}F^o)	–	3d (^{2}D^e)	426.7	A	8.06+1	5.65+1	3.72+1	2.73+1	2.14+1	1.79+1	1.51+1
				B	8.12+1	5.70+1	3.75+1	2.76+1	2.17+1	1.81+1	1.53+1
4f (^{2}F^o)	–	2s2p^2 (^{2}D^e)	106.4	A	5.22+0	3.66+0	2.40+0	1.76+0	1.39+0	1.16+0	9.76−1
				B	5.26+0	3.69+0	2.43+0	1.79+0	1.40+0	1.17+0	9.91−1
4d (^{2}D^e)	–	4p (^{2}P^o)	1784.7	A	2.95−1	2.30−1	1.71−1	1.37−1	1.16−1	1.03−1	9.58−2
				B	6.52+0	5.09+0	3.79+0	3.05+0	2.57+0	2.28+0	2.13+0
4d (^{2}D^e)	–	3p (^{2}P^o)	274.7	A	1.37+0	1.07+0	7.94−1	6.38−1	5.38−1	4.77−1	4.45−1
				B	3.03+1	2.37+1	1.76+1	1.42+1	1.19+1	1.06+1	9.90+0
4p (^{2}P^o)	–	2s2p^2 (^{2}D^e)	114.2	A	4.82+0	4.08+0	3.40+0	3.01+0	2.76+0	2.60+0	2.45+0
				B	1.25+1	1.03+1	8.24+0	7.02+0	6.24+0	5.74+0	5.45+0
3d (^{2}D^e)	–	3p (^{2}P^o)	723.5	A	2.02+0	1.48+0	1.03+0	7.91−1	6.57−1	5.86−1	5.66−1
				B	1.42+2	1.04+2	7.25+1	5.59+1	4.65+1	4.15+1	4.00+1
3p (^{2}P^o)	–	3s (^{2}S^e)	658.0	A	9.39+0	7.82+0	6.57+0	6.20+0	6.28+0	6.56+0	7.21+0
				B	7.19+1	5.50+1	4.04+1	3.29+1	2.88+1	2.67+1	2.67+1
3p (^{2}P^o)	–	2s2p^2 (^{2}D^e)	176.2	A	1.11+1	9.23+0	7.75+0	7.31+0	7.41+0	7.73+0	8.50+0
				B	8.48+1	6.48+1	4.77+1	3.88+1	3.39+1	3.15+1	3.14+1
3p (^{2}P^o)	–	2s2p^2 (^{2}S^e)	284.1	A	9.42+0	7.85+0	6.60+0	6.22+0	6.31+0	6.58+0	7.24+0
				B	7.21+1	5.52+1	4.06+1	3.30+1	2.89+1	2.68+1	2.68+1
3s′ (^{2}P^o)	–	2s2p^2 (^{2}S^e)	123.2	A	2.56+0	2.13+0	1.77+0	1.62+0	1.55+0	1.51+0	1.50+0
				B	4.18+0	3.46+0	2.82+0	2.50+0	2.31+0	2.21+0	2.22+0
2s2p^2 (^{2}D^e)	–	2s^{2}2p (^{2}P^o)	133.5	A	8.18+2	7.15+2	5.41+2	4.24+2	3.48+2	2.96+2	2.32+2
2s2p^2 (^{2}S^e)	–	2s^{2}2p (^{2}P^o)	103.7	A	7.74+1	8.63+1	8.19+1	7.40+1	6.72+1	6.18+1	5.39+1
2p^3 (^{2}P^o)	–	2s2p^2 (^{2}D^e)	106.6	A	4.06+0	3.40+0	2.75+0	2.39+0	2.18+0	2.06+0	2.05+0
				B	8.05+0	6.87+0	5.61+0	4.87+0	4.42+0	4.15+0	4.11+0

Table 4. Effective recombination coefficients [10^{-14} cm^3 s^{-1}] for temperature range $T_e = 500 - 2500$ K. Electron density $N_e = 10^4$ [cm^{-3}]

Transition			λ[nm]	Case	T_e [1000 K] 0.50	0.75	1.00	1.25	1.50	2.00	2.50
8h (^{2}H^o)	–	6g (^{2}G^e)	1866.2	A	2.07+1	1.45+1	1.12+1	9.22+0	7.83+0	6.02+0	4.88+0
8h (^{2}H^o)	–	5g (^{2}G^e)	931.4	A	1.88+1	1.31+1	1.02+1	8.36+0	7.10+0	5.46+0	4.43+0
7h (^{2}H^o)	–	6g (^{2}G^e)	3068.8	A	5.28+1	3.63+1	2.79+1	2.26+1	1.91+1	1.44+1	1.16+1
7h (^{2}H^o)	–	5g (^{2}G^e)	1157.9	A	5.05+1	3.47+1	2.66+1	2.16+1	1.82+1	1.38+1	1.11+1
7g (^{2}G^e)	–	5f (^{2}F^o)	1144.4	A	2.15+1	1.53+1	1.21+1	1.01+1	8.71+0	6.85+0	5.67+0
7g (^{2}G^e)	–	4f (^{2}F^o)	534.2	A	2.58+1	1.84+1	1.46+1	1.21+1	1.04+1	8.22+0	6.80+0
7f (^{2}F^o)	–	3d (^{2}D^e)	237.5	A	1.34+1	9.86+0	8.01+0	6.84+0	6.01+0	4.91+0	4.18+0
				B	1.36+1	1.00+1	8.12+0	6.93+0	6.10+0	4.98+0	4.25+0
7d (^{2}D^e)	–	3p (^{2}P^o)	179.6	A	1.08+0	8.22−1	6.90−1	6.12−1	5.61−1	4.93−1	4.48−1
				B	1.12+1	8.47+0	7.11+0	6.31+0	5.78+0	5.08+0	4.61+0
6h (^{2}H^o)	–	5g (^{2}G^e)	1851.6	A	2.31+2	1.54+2	1.16+2	9.21+1	7.63+1	5.63+1	4.42+1
6g (^{2}G^e)	–	5f (^{2}F^o)	1819.9	A	5.46+1	3.83+1	2.99+1	2.47+1	2.10+1	1.63+1	1.33+1
6g (^{2}G^e)	–	4f (^{2}F^o)	646.2	A	7.05+1	4.95+1	3.87+1	3.19+1	2.72+1	2.11+1	1.72+1
6f (^{2}F^o)	–	4d (^{2}D^e)	615.1	A	1.70+1	1.25+1	1.01+1	8.53+0	7.46+0	6.04+0	5.12+0
				B	1.72+1	1.26+1	1.02+1	8.64+0	7.56+0	6.13+0	5.20+0
6f (^{2}F^o)	–	3d (^{2}D^e)	257.5	A	2.85+1	2.08+1	1.68+1	1.43+1	1.25+1	1.01+1	8.56+0
				B	2.88+1	2.11+1	1.70+1	1.44+1	1.26+1	1.02+1	8.69+0
6d (^{2}D^e)	–	3p (^{2}P^o)	191.0	A	1.84+0	1.40+0	1.16+0	1.01+0	9.06−1	7.67−1	6.76−1
				B	2.12+1	1.61+1	1.34+1	1.16+1	1.04+1	8.84+0	7.79+0
5g (^{2}G^e)	–	4f (^{2}F^o)	990.3	A	3.46+2	2.35+2	1.79+2	1.44+2	1.21+2	9.05+1	7.21+1
5f (^{2}F^o)	–	4d (^{2}D^e)	923.0	A	4.35+1	3.13+1	2.49+1	2.09+1	1.81+1	1.44+1	1.21+1
				B	4.39+1	3.16+1	2.52+1	2.11+1	1.83+1	1.46+1	1.22+1
5f (^{2}F^o)	–	3d (^{2}D^e)	299.3	A	8.35+1	6.01+1	4.78+1	4.01+1	3.48+1	2.77+1	2.32+1
				B	8.42+1	6.06+1	4.83+1	4.06+1	3.52+1	2.80+1	2.35+1
5d (^{2}D^e)	–	3p (^{2}P^o)	213.8	A	3.17+0	2.38+0	1.97+0	1.71+0	1.52+0	1.28+0	1.11+0
				B	4.35+1	3.27+1	2.70+1	2.34+1	2.09+1	1.75+1	1.53+1
4f (^{2}F^o)	–	3d (^{2}D^e)	426.7	A	4.83+2	3.35+2	2.58+2	2.11+2	1.79+2	1.37+2	1.11+2
				B	4.85+2	3.36+2	2.60+2	2.12+2	1.80+2	1.38+2	1.12+2
4f (^{2}F^o)	–	2s2p^2 (^{2}D^e)	106.4	A	3.13+1	2.16+1	1.67+1	1.37+1	1.16+1	8.88+0	7.21+0
				B	3.14+1	2.17+1	1.68+1	1.37+1	1.16+1	8.94+0	7.25+0
4d (^{2}D^e)	–	4p (^{2}P^o)	1784.7	A	1.13+0	8.40−1	6.85−1	5.88−1	5.20−1	4.29−1	3.70−1
				B	2.50+1	1.85+1	1.51+1	1.30+1	1.15+1	9.49+0	8.18+0
4d (^{2}D^e)	–	3p (^{2}P^o)	274.7	A	5.26+0	3.90+0	3.18+0	2.73+0	2.42+0	1.99+0	1.72+0
				B	1.16+2	8.61+1	7.03+1	6.04+1	5.34+1	4.41+1	3.80+1
4p (^{2}P^o)	–	2s2p^2 (^{2}D^e)	114.2	A	1.44+1	1.10+1	9.20+0	8.10+0	7.33+0	6.32+0	5.66+0
				B	3.90+1	2.94+1	2.45+1	2.15+1	1.95+1	1.67+1	1.49+1
3d (^{2}D^e)	–	3p (^{2}P^o)	723.5	A	1.03+1	7.30+0	5.74+0	4.77+0	4.11+0	3.24+0	2.69+0
				B	7.18+2	5.08+2	4.00+2	3.33+2	2.87+2	2.26+2	1.88+2
3p (^{2}P^o)	–	3s (^{2}S^e)	658.0	A	3.02+1	2.29+1	1.90+1	1.66+1	1.49+1	1.27+1	1.12+1
				B	3.16+2	2.28+2	1.82+2	1.54+2	1.34+2	1.09+2	9.22+1
3p (^{2}P^o)	–	2s2p^2 (^{2}D^e)	176.2	A	3.57+1	2.70+1	2.24+1	1.96+1	1.76+1	1.50+1	1.32+1
				B	3.73+2	2.69+2	2.15+2	1.81+2	1.58+2	1.28+2	1.09+2
3p (^{2}P^o)	–	2s2p^2 (^{2}S^e)	284.1	A	3.04+1	2.30+1	1.91+1	1.67+1	1.50+1	1.27+1	1.13+1
				B	3.17+2	2.29+2	1.83+2	1.54+2	1.35+2	1.09+2	9.25+1
3s′ (^{2}P^o)	–	2s2p^2 (^{2}S^e)	123.2	A	7.77+0	5.91+0	4.94+0	4.35+0	3.94+0	3.40+0	3.04+0
				B	1.25+1	9.50+0	7.97+0	7.04+0	6.39+0	5.54+0	4.96+0
2s2p^2 (^{2}D^e)	–	2s^{2}2p (^{2}P^o)	133.5	A	1.99+2	2.02+2	2.94+2	4.22+2	5.46+2	7.22+2	8.06+2
2s2p^2 (^{2}S^e)	–	2s^{2}2p (^{2}P^o)	103.7	A	4.15+1	3.16+1	2.76+1	2.79+1	3.16+1	4.45+1	5.84+1
2p^3 (^{2}P^o)	–	2s2p^2 (^{2}D^e)	106.6	A	1.11+1	8.40+0	7.07+0	6.29+0	5.79+0	5.14+0	4.70+0
				B	1.91+1	1.46+1	1.24+1	1.13+1	1.06+1	9.72+0	9.09+0

Table 5. Polynomial fitting for effective recombination coefficients at electron density $N_e = 10^4$ [cm^{-3}]. Temperature range $T_e = 5000 - 20\,000$ K

Transition			λ[nm]	Case	a	b	c	d	f	%
8h (^{2}H^o)	–	6g (^{2}G^e)	1866.2	A	1.134	−0.878	−0.134	−0.033	−2.0410	0.00
8h (^{2}H^o)	–	5g (^{2}G^e)	931.4	A	1.029	−0.878	−0.134	−0.033	−2.0409	0.00
7h (^{2}H^o)	–	6g (^{2}G^e)	3068.8	A	2.506	−0.911	−0.113	−0.024	−2.1160	0.00
7h (^{2}H^o)	–	5g (^{2}G^e)	1157.9	A	2.395	−0.911	−0.113	−0.024	−2.1160	0.00
7g (^{2}G^e)	–	5f (^{2}F^o)	1144.4	A	1.530	−0.324	−0.188	−0.185	−1.3745	0.05
7g (^{2}G^e)	–	4f (^{2}F^o)	534.2	A	1.836	−0.324	−0.188	−0.185	−1.3746	0.05
7f (^{2}F^o)	–	3d (^{2}D^e)	237.5	A	1.422	0.037	−0.009	−0.251	−0.8371	0.39
				B	1.450	0.037	−0.007	−0.252	−0.8334	0.39
7d (^{2}D^e)	–	3p (^{2}P^o)	179.6	A	0.208	−0.084	−0.048	−0.186	−0.7186	0.07
				B	2.143	−0.083	−0.048	−0.187	−0.7186	0.07
6h (^{2}H^o)	–	5g (^{2}G^e)	1851.6	A	8.528	−0.948	−0.083	−0.015	−2.2204	0.00
6g (^{2}G^e)	–	5f (^{2}F^o)	1819.9	A	3.320	−0.304	−0.174	−0.190	−1.4071	0.05
6g (^{2}G^e)	–	4f (^{2}F^o)	646.2	A	4.290	−0.304	−0.174	−0.190	−1.4071	0.05
6f (^{2}F^o)	–	4d (^{2}D^e)	615.1	A	1.661	0.023	−0.017	−0.243	−0.8835	0.34
				B	1.695	0.021	−0.016	−0.243	−0.8800	0.34
6f (^{2}F^o)	–	3d (^{2}D^e)	257.5	A	2.778	0.023	−0.017	−0.243	−0.8835	0.34
				B	2.834	0.021	−0.016	−0.243	−0.8800	0.34
6d (^{2}D^e)	–	3p (^{2}P^o)	191.0	A	0.288	−0.085	−0.059	−0.187	−0.7652	0.12
				B	3.315	−0.083	−0.058	−0.188	−0.7634	0.13
5g (^{2}G^e)	–	4f (^{2}F^o)	990.3	A	15.451	−0.309	−0.154	−0.190	−1.5065	0.04
5f (^{2}F^o)	–	4d (^{2}D^e)	923.0	A	3.585	−0.003	−0.028	−0.230	−0.9691	0.27
				B	3.649	−0.004	−0.028	−0.229	−0.9656	0.27
5f (^{2}F^o)	–	3d (^{2}D^e)	299.3	A	6.878	−0.003	−0.028	−0.230	−0.9691	0.27
				B	7.001	−0.004	−0.028	−0.229	−0.9656	0.27
5d (^{2}D^e)	–	3p (^{2}P^o)	213.8	A	0.454	−0.089	−0.058	−0.187	−0.7970	0.11
				B	6.247	−0.086	−0.056	−0.189	−0.7936	0.11
4f (^{2}F^o)	–	3d (^{2}D^e)	426.7	A	27.273	−0.053	−0.039	−0.209	−1.1448	0.15
				B	27.586	−0.055	−0.039	−0.208	−1.1416	0.15
4f (^{2}F^o)	–	2s2p^2 (^{2}D^e)	106.4	A	1.765	−0.053	−0.039	−0.209	−1.1448	0.15
				B	1.785	−0.055	−0.039	−0.208	−1.1416	0.15
4d (^{2}D^e)	–	4p (^{2}P^o)	1784.7	A	0.137	−0.067	−0.027	−0.211	−0.8425	0.09
				B	3.047	−0.066	−0.026	−0.212	−0.8391	0.09
4d (^{2}D^e)	–	3p (^{2}P^o)	274.7	A	0.638	−0.067	−0.027	−0.211	−0.8424	0.09
				B	14.150	−0.066	−0.026	−0.212	−0.8391	0.09
4p (^{2}P^o)	–	2s2p^2 (^{2}D^e)	114.2	A	3.014	−0.643	−0.054	−0.092	−1.0502	0.01
				B	7.022	−0.231	−0.042	−0.144	−0.7814	0.03
3d (^{2}D^e)	–	3p (^{2}P^o)	723.5	A	0.791	−0.508	0.036	−0.341	−1.3973	0.01
				B	55.869	−0.494	0.032	−0.336	−1.3773	0.01
3p (^{2}P^o)	–	3s (^{2}S^e)	658.0	A	6.201	−0.304	0.412	0.215	−0.3676	0.13
				B	32.883	−0.752	0.140	−0.281	−1.4218	0.02
3p (^{2}P^o)	–	2s2p^2 (^{2}D^e)	176.2	A	7.312	−0.304	0.412	0.215	−0.3676	0.13
				B	38.774	−0.752	0.140	−0.281	−1.4218	0.02
3p (^{2}P^o)	–	2s2p^2 (^{2}S^e)	284.1	A	6.224	−0.304	0.412	0.215	−0.3676	0.13
				B	33.006	−0.752	0.140	−0.281	−1.4217	0.02
3s$'$ (^{2}P^o)	–	2s2p^2 (^{2}S^e)	123.2	A	1.619	−0.982	0.196	−0.019	−1.2415	0.09
				B	2.495	−0.487	0.041	−0.105	−0.8786	0.20
2s2p^2 (^{2}D^e)	–	2s^{2}2p (^{2}P^o)	133.5	A	423.926	−1.353	0.167	−0.047	−2.2304	0.02
2s2p^2 (^{2}S^e)	–	2s^{2}2p (^{2}P^o)	103.7	A	73.955	−1.477	0.217	0.006	−1.8827	0.02
2p^3 (^{2}P^o)	–	2s2p^2 (^{2}D^e)	106.6	A	2.387	−0.228	0.046	−0.107	−0.6876	0.09
				B	4.873	−0.163	0.022	−0.122	−0.6327	0.08

treatment described by Storey (1994) and Kisielius et al. (1998).

In Table 3, we give the effective recombination coefficients $\alpha_{\rm eff}(\lambda)$ for the strongest recombination lines of C II for the temperature range $3\,500 - 20\,000$ K. Only the lines with the $\alpha_{\rm eff}(\lambda) \geq 3.0\,10^{-14}$ cm^{3}s^{-1} and $\lambda > 91.2$ nm at one or more temperatures are presented. Table 3 is a specimen table showing only the strongest lines. More extensive tables showing weaker lines are available in electronic form from the CDS.

The effective recombination coefficient is defined such that the emissivity $\epsilon(\lambda)$, in a transition of wavelength λ is

$$\epsilon(\lambda) = N_{\rm e} N_+ \alpha_{\rm eff}(\lambda) \frac{hc}{\lambda} \ \ [\mathrm{ergs\,cm^{-3}\ s^{-1}}]. \qquad (2)$$

We tabulate results for a single value of electron density $N_{\rm e} = 10^4$ cm^{-3} because the recombination coefficients are not very sensitive to this parameter at low temperature.

The effective recombination coefficients $\alpha_{\rm eff}(\lambda)$ for the lower temperatures $T_{\rm e} = 500 - 2\,500$ K are presented in Table 4 for the same set of lines as given in Table 3. Once again the reader is referred to the electronic version of this paper at the CDS for more extensive tabulations.

Subsequently, the coefficients were fitted by a least-squares algorithm to the functional form

$$\alpha_{\rm eff} = 10^{-14}\, a\, t^f \times \left(1 + b\,(1-t) + c\,(1-t)^2 + d\,(1-t)^3\right), \qquad (3)$$

where $t = T_{\rm e}[K]/10^4$, and a, b, c, d and f are constants.

We present the coefficients of the fits to the recombination coefficients in Table 5 for the same set of lines as given in Table 3. The fitting accuracy (the maximum error of fitting in percent) is also given. This gives an indication that fitting is very accurate for the temperature range ($5000 - 20\,000$ K) considered here. Due to the more complex nature of recombination at lower temperatures caused by the interaction of dielectronic and radiative recombination, fits were not made for lower temperatures. Fit coefficients for a more extensive set of lines are available from the CDS.

As part of a calculation of total electron-ion recombination coefficients for a range of atomic ions, Nahar (1995) reported state-specific recombination coefficients for some states of C^+, derived from photoionization data calculated using similar methods to those used in the present work. The numbers given by Nahar are for direct recombination to each state, no cascade contributions are included. In Table 6 we compare the results of Nahar at $T_{\rm e} = 1\,000$ K with the present work. For Rydberg states with $l \geq 2$ we find good agreement with Nahar, with differences of $\leq 5\%$ for d-states and $\leq 1\%$ for f-states. For the $2s2p^2\ ^2D^e$ state our recombination coefficient is about twice that found by Nahar. The recombination to this state is dominated by near-threshold resonances, whose position we have empirically adjusted downwards to agree with the experimental position, leading to a larger recombination coefficient, which is also in good agreement with that given by Nussbaumer & Storey (1983) for this state. The most significant difference between our work and that of Nahar is for the $^2P^o$ states. In the work of Nahar, the state with the largest direct recombination coefficient is given as $2p^3\ ^2P^o$, while we find this state to have a recombination coefficient two orders of magnitude smaller than that given by Nahar. We note, however that the value given by Nahar for this state is close to the value we find for the ground $2s^22p\ ^2P^o$ state, and similarly for the $2s^22p\ ^2P^o$ state of Nahar and our $2s^23p\ ^2P^o$ state. The same pattern is also found for higher members of the $^2P^o$ series. We conclude that the order of the identification of the $^2P^o$ states given in Table 2 of Nahar is incorrect, although their contribution to the total recombination coefficient is not affected and broadly similar to that in the present work.

In Table 7 we compare our effective recombination coefficients for some strong lines with the list given in

Table 6. Comparison of state-specific recombination coefficients [10^{-13} cm^3 s^{-1}] with data from Nahar (1995) at electron density $N_{\rm e} = 10^4$ [cm^{-3}] and temperature $T_{\rm e} = 10\,000$ K

State		Nahar	Present
$2p^3$	$^2P^o$	36.2	0.4
$2s2p^2$	^2D	10.8	21.0
$2s^23d$	^2D	4.2	3.7
$2s^22p$	$^2P^o$	4.1	36.6
$2s^24d$	^2D	2.6	2.7
$2s^24f$	$^2F^o$	1.7	1.7
$2s^25d$	^2D	1.6	1.7
$2s^25f$	$^2F^o$	1.6	1.6
$2s^23p$	$^2P^o$	1.2	3.9
$2s^24p$	$^2P^o$	–	1.0

Table 7. Comparison of effective recombination coefficients [10^{-13} cm^3 s^{-1}] with data from Pèquignot et al. (1991) (PPB) at electron density $N_{\rm e} = 10^4$ [cm^{-3}] and temperature $T_{\rm e} = 10\,000$ K

Transition			λ[nm]	Case	Present	PPB
5g (^{2}G)	–	4f (^{2}F^o)	990.3	A	1.545	1.621
4f (^{2}F^o)	–	3d (^{2}D)	426.7	A	2.727	2.795
3d (^{2}D)	–	3p (^{2}P^o)	723.5	A	0.079	0.065
				B	5.587	5.184
3p (^{2}P^o)	–	3s (^{2}S)	658.0	A	0.620	0.329
				B	3.288	1.444
3p (^{2}P^o)	–	2s2p^2 (^{2}S)	284.1	A	0.622	0.606
				B	2.658	3.301
3p (^{2}P^o)	–	2s2p^2 (^{2}D)	176.2	A	0.731	1.001
				B	3.877	4.391
2s2p^2 (^{2}D)	–	2p (^{2}P^o)	133.5	A	42.39	3.450

Pèquignot et al. (1991) (PPB). There is reasonably good agreement for lines originating from the 5g, 4f and 3d states. At first sight the agreement is significantly worse for the lines originating from the 3p ^{2}P^o state. Most of the difference, however, arises from the branching ratios from the 3p ^{2}P^o state to lower states. In Case A, the total $\alpha_{\rm eff}$ for this state is 1.973 10^{-13} from our data and 1.936 10^{-13} from PPB. In Case B the the corresponding values are 10.466 10^{-13} and 8.493 10^{-13}, a difference of 23%. In Case B, most of the recombination to the nd series passes through the 3p state rather than going directly to the ground 2p state. A possible cause of the difference in the Case B results is that the nd series is truncated at some relatively low principal quantum number in PPB, whereas in our calculation the infinite series of nd states is included.

The differences in the effective recombination coefficients for individual lines from the 3p ^{2}P^o can be explained by differences in the branching ratios, β, from the 3p ^{2}P^o state to lower states. In our calculation we have β(3s ^{2}S^e) = 0.314, β(2s2p^2 ^{2}S^e) = 0.315 and β(2s2p^2 ^{2}D^e) = 0.371 while PPB give these parameters as 0.170, 0.313 and 0.517. We note that our values of β are in reasonable agreement with data retrieved from the Opacity Project data base (Cunto et al. 1993) which give 0.311, 0.311 and 0.378 respectively.

The difference in $\alpha_{\rm eff}$ for the line 2s2p^2 ^{2}D^e – 2s^{2}2p ^{2}P^o arises from dielectronic recombination being not included in PPB. Here our coefficient is in good agreement with the purely dielectronic coefficient $\alpha_{\rm DR}$ = 45.36 10^{-13} from Nussbaumer & Storey (1983).

5. Conclusions

The energy levels of C^+ doublet bound states with $n \leq 15$, $L \leq 4$ were calculated using the R-matrix method. Photoionization cross-sections for these states were computed using a variable step energy mesh ensuring the correct mapping of resonances. The importance of correctly delineating the autoionizing resonances in the photoionization cross-sections was demonstrated by considering the area under the cross-section. In the case of 2s2p^2 ^{2}D^e, this area differs by factor of 3 comparing our data with those from the OP (Yu Yan & Seaton 1987).

We find that moving the two energetically lowest resonances to the experimental positions in the appropriate cross-sections significantly increases their contribution to the recombination coefficients, particularly at low temperatures.

The effective recombination coefficients for lines of C II have been tabulated in the temperature range $T_{\rm e}$ = 500−20 000 K and at electron density $N_{\rm e} = 10^4$ cm^{-3}. The use of atomic data of high quality for bound-bound and bound-free radiative processes among all the terms with $n \leq 15$ means that the results given here are expected to be more reliable than any previous work.

References

Badnell N.R., 1988, J. Phys. B 21, 749
Berrington K.A., Burke P.G., Dufton P.L., Kingston A.E., 1977, J. Phys. B 10, 1465
Berrington K.A., Burke P.G., Butler K., Seaton M.J., Storey P.J., Taylor K.T., Yu Yan, 1987, J. Phys. B 20, 6379
Cunto W., Mendoza C., Ochsenbein F., Zeippen C.J., 1993, J. Phys. B 4, 314
DeMarco O., Storey P.J., Barlow M.J., 1998, MNRAS 291, 999
Fano U., 1961, Phys. Rev. 124, 1866
Ferland G.J., Williams R.E., Lambert D.L., Shields G.A., Slovak M., Gondhalekar P.M., Truran J.W., 1984, ApJ 281, 194
Hibbert A., 1975, Comput. Phys. Commun. 9, 141
Kisielius R., Storey P.J., Davey A.R., Neale L., 1998, A&AS 133, 257
Liu X.-W., Storey P.J., Barlow M.J., Danziger I.J., Cohen M., Bryce M., 2000, MNRAS (in press)
Moore C.E., 1970, "Atomic Energy Levels", National Bureau of Standards, U.S.A.
Nahar S., 1995, ApJS 101, 423
Nussbaumer H., Storey P.J., 1983, A&A 126, 75
Péquignot D., Petitjean P., Boisson C., 1991, A&A 251, 680
Seaton M.J., 1987, J. Phys. B 20, 6363
Storey P.J., 1981, MNRAS 195, 27
Storey P.J., 1982, Planetary Nebulae IAU Symposium, No. 103, 199
Storey P.J., 1994, A&A 282, 999
Yu Yan, Seaton M.J., 1987, J. Phys. B 20, 6409